Physica B 717 (2025) 417802

Contents lists available at ScienceDirect

Physica B: Condensed Matter

journal homepage: www.elsevier.com/locate/physb

Enhanced photocatalytic degradation of diazo reactive blue 198 using ternary PANI-TiO_2-CuO composites: Predicted degradation pathway, mechanism, and DFT calculations

Nazli Turkten [a], Yunus Karatas [a,*], Simal Kurumoglu [b], Yelda Yalcin Gurkan [b]

[a] Department of Chemistry, Faculty of Arts and Sciences, Kirsehir Ahi Evran University, Kirsehir, 40100, Türkiye
[b] Department of Chemistry, Faculty of Arts and Sciences, Tekirdag Namik Kemal University, Tekirdag, 59030, Türkiye

ARTICLE INFO

Keywords:
Conceptual density functional theory
PANI-TiO_2-CuO composites
Photocatalysis
Reactive blue 198
Recyclability tests
Silico toxicity

ABSTRACT

This study investigated the preparation and detailed characterization of PANI (polyaniline)-TiO_2-CuO composites through in-situ chemical oxidation polymerization (PTCI) and mechano-chemical synthesis (PTCS) methods for comparison. The morphological characteristics of ternary composites depend on the ratios of PANI to binary TiO_2-CuO composite and the process of preparation. The photocatalytic degradation of diazo Reactive Blue 198 (RB-198) in the presence of the PTCS-81 composite (PANI: TiO_2-CuO composite with a mole ratio of 8:1, prepared using PTCS method) reached 90.4 % within 60 min. Recyclability tests revealed that the composites are stable, underscoring their potential as effective photocatalysts. The proposed degradation pathways of diazo RB-198 dye were discussed both experimentally and theoretically for the first time. The reactivity descriptors confirmed that the nitrogen atoms were favorably sensitive sites for radical attacks. Finally, the silico toxicity of potential photodegraded products of RB-198 was assessed via the computational toxicology method ProTox-3.0.

1. Introduction

The expansion of the textile industry contributes significantly to water pollution due to high-water consumption and the improper discharge of dye materials into wastewater. Azo dyes are easy to synthesize, have high fastness ratings, and exhibit good solubility properties, making them widely found in wastewater from textile manufacturing. A pivotal global assessment is essential to minimize the catastrophic impacts of textile wastewater on human health and aquatic ecosystems, focusing on environmentally friendly treatment solutions. Heterogeneous photocatalysis is a promising advanced oxidation process for large-scale applications that effectively degrade azo dyes in wastewater [1–4].

Recently, advances in photocatalysis have been significantly driven by conducting polymer-based composites, particularly PANI [3,5]. Excellent environmental stability, low cost, and ease of preparation make PANI a preferred choice in conducting polymers. The combination of PANI with metal oxides is an efficient photocatalyst, featuring π and σ bond systems and synergistic properties that degrade dyes through surface modification [6,7].

So far, various metal oxides with distinct properties have been incorporated into PANI to achieve PANI-based composites as photocatalysts. Among them, TiO_2 and ZnO are the primary metal oxides that couple with PANI, standing out PANI-TiO_2 and PANI-ZnO composites, which exhibit enhanced photocatalytic performance [5,8,9]. Compared to these surface-modified composite strategies, the design of CuO and CuO-TiO_2 component systems with PANI is a promising new candidate in photocatalysis [10–15].

PANI-based composites are mainly synthesized via an *in-situ* chemical oxidation method. In this method, aniline (ANI) is chemically oxidized in a strongly acidic medium with a free radical initiator oxidant, such as ammonium peroxydisulfate. However, mechano-chemical preparation is a cost-effective alternative process option in a low pH medium to address the dissolution issue of CuO. Turkten et al. prepared PANI-CuO composites using *in-situ* chemical oxidation polymerization and mechano-chemical methods for highly enhanced photocatalytic degradation of an anionic textile dye [10]. They reported that the CuO amount in composites and synthesis route played a critical role in the morphological, structural, optical, and surface features of PANI-CuO composites. In another photocatalytic study, the catalytic

* Corresponding author.
E-mail addresses: nazli.turkten@ahievran.edu.tr (N. Turkten), ykaratas@ahievran.edu.tr (Y. Karatas), skurumoglu@nku.edu.tr (S. Kurumoglu), yyalcin@nku.edu.tr (Y. Yalcin Gurkan).

https://doi.org/10.1016/j.physb.2025.417802
Received 28 June 2025; Received in revised form 5 September 2025; Accepted 10 September 2025
Available online 16 September 2025

activity of iron-doped PANI-CuO composites was tested on methylene blue (MB) and Cr(VI) [12]. Photocatalytic degradation of MB dye was investigated using boron-doped PANI-CuO composites, prepared by a simple solution combustion method [13]. Lately, extensive research has focused on preparing ternary PANI-based composites that reduce photogenerated electron-hole recombination and demonstrate superior photocatalytic performance [11,16,17]. Ternary PANI-CuO composites such as chitosan/hydroxyethyl cellulose gel immobilized PANI-CuO-ZnO hybrid nanocomposite [15] and chitosan-PANI-CuO nanocomposite [14] were synthesized for photocatalytic degradation of dyes.

Radicals are formed in photocatalysis to react with organic pollutants to break them down into smaller, less harmful compounds. Analysis of Fukui indices from density functional theory (DFT) indicates localized reactive sites responsible for organic pollutants, and comprehending this process helps explain experimental observations. Therefore, predicting the photocatalytic degradation mechanism of organic pollutants is crucial in integrated theoretical-experimental studies [18,19]. In this approach, the photocatalytic degradation mechanism of pharmaceuticals and dyes using various catalysts was proposed by combining experimental and theoretical approaches [10,20,21]. The photocatalytic mechanism of the antibiotic cefazolin [20] and the azo dye Reactive Red-195 [21] was elucidated using a TiO_2 photocatalyst. Then, Turkten et al. studied the polyaniline (PANI)-CuO composites for the predicted degradation mechanism and pathways of anionic Reactive Orange-122 dye [10].

Numerous studies have been performed to design p-n-p type photocatalytic heterojunction structures by combining p-type (such as CuO, Cu_2O, etc.) with n-type (such as TiO_2, ZnO, etc.) semiconductors and subsequently introducing PANI (p-type) conducting polymer [11,16,17]. Borik et al. prepared a TiO_2-PANI-Cu_2O ternary nanocomposite, and its photocatalytic performance was evaluated for the decomposition of methyl orange under visible light irradiation [16]. In another study, the photocatalytic property of p-n-p type CuO-ZnO-PANI nanocomposite was evaluated by the degradation of 4-chlorophenol [17]. However, there is only one experimental study reported on the preparation of CuO-TiO_2-PANI nanocomposite as a photocatalyst to investigate the degradation of chlorpyrifos [11].

Considering the gap in p-n-p type photocatalytic performance, combined experimental and theoretical investigations were conducted for the first time on PANI-TiO_2-CuO composite. To address the effects of different molar ratios and preparation methods on the structural, morphological, thermal, and surface properties of ternary PANI-TiO_2-CuO composites, a series of these composites was synthesized using *in-situ* chemical oxidation polymerization and mechano-chemical routes. For the first time, a theoretical and experimental proposal for the photocatalytic mechanism of Reactive Blue 198 (RB-198), assisted by hydroxyl radicals, was conducted. DFT-based reaction descriptors in the form of Fukui functions were used to describe the predicted reaction pathways RB-198, and theoretical findings were supported by experimental spectral results and literature. It is essential to assess the toxicity of predicted compounds in the field of water depollution of RB-198. In this context, a silico toxicity analysis was conducted on the compounds formed through the proposed degradation mechanism of RB-198 to evaluate their toxicological impact, which is a significant aspect of this study. Finally, the reusability and recycling properties of ternary PANI-TiO_2-CuO composites were investigated, then characterized with FTIR-ATR -ATR (Fourier transform infrared spectroscopy equipped with an attenuated total reflection accessory) and XRD (X-ray diffraction) analysis.

2. Methodology

2.1. Materials

Copper (II) oxide (CuO, ACS, ≥99 %, Thermo Scientific), TiO_2 (Evonik, P-25), ANI ($C_6H_5NH_2$, for analysis, ≥99.5 %, Merck)), ammonium persulfate (APS, $(NH_4)_2S_2O_8$, ACS, ≥98.0 %, Merck), hydrochloric acid (HCl, ACS, 37 %, Merck), and RB-198($C_{41}H_{30}Cl_4N_{14}Na_4O_{14}S$, Birkim Textile) were used as received without further purification. Polyaniline emeraldine salt (referred to as PANI) was prepared via *in-situ* chemical oxidation polymerization method as described in our previous study [8].

2.2. Binary TiO_2-CuO composite

Binary TiO_2-CuO composite was synthesized by a mechanical mixing method with a minor modification [22]. In this cost-effective procedure, TiO_2 (1 g) and CuO (1 g) were mixed in ethanol (10 mL) in a mortar for 10 min, sonicated in an ultrasonic bath for 30 min, dried at 105 °C for 24 h, and calcined at 500 °C for 5 h.

2.3. Preparation of ternary PANI-TiO_2-CuO composites

Ternary PANI-TiO_2-CuO composites were prepared via the mechano-chemical preparation method, referred to as PTCS-PANI composites, and *in-situ* chemical oxidation polymerization method, referred to as PTCI-PANI composites with a minor modification [10].

A mechano-chemical preparation method was adopted to prepare three different stoichiometric amounts of PTCS-PANI composites from synthesized PANI and binary TiO_2-CuO composite (as detailed above). The mole ratios of PANI:TiO_2-CuO were 1:8, 1:1, and 8:1, and these PTCS-PANI composites were labeled as PTCS-18, PTCS-11, and PTCS-81, respectively. Briefly, an appropriate amount of p-type (PANI) and n-p type (TiO_2-CuO) materials were added into a beaker, mixed in distilled water (50 mL), and stirred continuously for 24 h. After that, the mixture was filtered, washed with distilled water, and dried at 80 °C for 24 h.

The *in-situ* chemical oxidation polymerization method involves the oxidative polymerization of aniline monomer using ammonium persulphate as the initiator along with acid dopants, preferably using an HCl solution. The fact that CuO dissolves in acidic solutions has been ignored in several studies. PTCI-PANI composites were synthesized with the initial mole ratio of ANI:APS being 1:1 in all composites. The mole ratios of ANI:TiO_2-CuO were initially 1:8, 1:1, and 8:1, and these ternary composites were named PTCI-18, PTCI-11, and PTCI-81, respectively. The representative preparation of PTCI-11 was outlined as follows: Initially, 5.71 g (25 mmol) of APS was evenly dispersed in a beaker containing 80 mL of 1 M HCl solution (Solution A). This solution was then carefully transferred into a dropping funnel. 2.0 g of binary TiO_2-CuO composite was added to 80 mL of 1 M HCl solution (Solution B), followed by ultrasonication for 15 min. Subsequently, Solution B was placed in an ice bath, and 2.33 g (25 mmol) of ANI was poured slowly under continuous vigorous stirring. A dropwise addition of Solution A to Solution B was performed by vigorous stirring, and the mixture was kept under magnetic stirring for an additional 24 h at room temperature. Finally, the product was filtered and washed with distilled water and dried in an air oven at 80 °C for 24 h.

2.4. Photocatalyst characterization

FTIR-ATR spectra were observed using a Thermo Scientific Nicolet 6700 Spectrometer spanning a spectral range of 4000–500 cm^{-1}. All specimens were performed on 32 scans at a resolution of 4 cm^{-1}. A Rigaku-D/MAX-Ultima diffractometer was employed with Cu Kα radiation beam (λ = 1.54 Å) to conduct XRD analysis. The instrument operational parameters were 40 kV, 40 mA, and a scanning rate of 2° min^{-1}. The crystallite sizes of (D, nm) of binary TiO_2-CuO composite and ternary PANI-TiO_2-CuO composites were calculated using the Scherrer equation (Eq. (1)) related to $(\bar{1}\ 1\ 1)$ and (1 1 1) reflection planes of CuO and (1 0 1) and (2 0 0) planes of anatase TiO_2 [23].

$$D = K\lambda/(\beta \cos \theta) \quad (1)$$

where,

K: 0.9,

λ: X-ray wavelength (1.5418 Å),

θ: Bragg angle, and,

β: full width at half maximum intensity (FWHM, radians)

SEM analysis was carried out on a FEI-Philips XL30 Environmental Scanning Electron Microscope. Brunauer–Emmett–Teller (BET) surface property measurements were carried out on a Quantachrome Quadrosorb SI instrument. The specimens were degassed for 4 h before N_2 adsorption-desorption. Thermal profiles of photocatalysts were determined using a simultaneous TG (thermogravimetric)-DSC (differential scanning calorimetry) instrument (PerkinElmer model STA 600) under an inert pure N_2 atmosphere. The flow rate was set to 20 mL/min with a heating rate of 10 °C/min.

2.5. Photocatalytic activity experiments

The photocatalytic activity of binary TiO_2-CuO composite and three different ternary PTCS-PANI composites was evaluated by degrading RB-198 dye solution (10 mg/L) over an exposure time interval (t = 0–120 min). Each photocatalyst (0.25 mg/L) in RB-198 solution (50 mL) was excited from the top with a 125 W black light fluorescent lamp (λ_{max} = 365 nm). The aqueous suspension under irradiation was collected at certain intervals, filtered through a 0.22 μm membrane filter, and monitored by UV–vis (Ultraviolet–visible spectroscopy) analysis. The maximum wavelength of RB-198 was λ = 625 nm, and the percent removal of dye was presented as according to the equation:

$$\text{Decolorization } (\%) = ((A_o - A_t) \ / \ A_o) \text{ x } 100 \quad (2)$$

where A_o and A_t are the absorbances of RB-198 at the initial and time t, respectively.

2.6. Computational details

The Conceptual Density Functional Theory (CDFT)-based reactivity descriptor calculations between RB-198 dye and photogenerated hydroxyl radicals were employed in the Gaussian09 package [24] applying the B3LYP/6-31G(d) basis set [25,26]. Detailed information on the computational approach is available in our previous study [10]. The computational toxicity prediction of photodegraded products was employed by a web-based virtual software, ProTox 3.0 platform (https://tox.charite.de/protox3/) [27]. Further details are presented in the Supplementary Material (SM) in Part I.

3. Results and discussion

3.1. XRD analysis

XRD spectra of PANI, TiO_2-CuO, PTCS-PANI, and PTCI-PANI composites are shown in Fig. 1. The semi-crystalline peaks of PANI were observed as expected at 2θ = 8.99°, 15.42°, 20.34°, 25.30°, and 27.18°, which could be related to the (0 0 1), (0 1 1), (0 2 0), (2 0 0), and (1 2 1) reflection planes, respectively [28].

The XRD diffractogram of TiO_2-CuO revealed peaks at 2θ = 32.54°, 35.54°, 38.72°, 48.06°, 53.52°, 58.28°, 61.58°, 65.80°, 66.30°, 68.08°, and 72.42° attributed to (1 1 0), ($\bar{1}$ 1 1), (1 1 1), ($\bar{2}$ 0 2), (0 2 0), (2 0 2), ($\bar{1}$ 1 3), (0 2 2), ($\bar{3}$ 1 1), (2 2 0), and (3 1 1) planes of monoclinic CuO (JCPDS card no. 89–5895). The diffraction peaks of TiO_2 at 2θ = 25.30°, 36.97°, 37.84°, 48.80°, 53.92°, 55.14°, 62.72°, 68.94°, 70.34°, and 75.20° corresponded to (1 0 1), (1 0 3), (0 0 4), (2 0 0), (1 0 5), (2 1 1), (0 0 2), (1 1 6), (2 2 0), and (2 1 5), planes of anatase (JCPDS No. 73–1764), respectively. The other diffraction peaks of TiO_2 at 2θ = 27.44°, 36.12°, 41.26°, and 56.78° were assigned to (1 1 0), (1 0 1), (1 1 1), and (2 0 0) planes of rutile (JCPDS No. 99-0090), respectively. The combination signals from TiO_2 and CuO indicated a successful dual-phase TiO_2-CuO composite preparation.

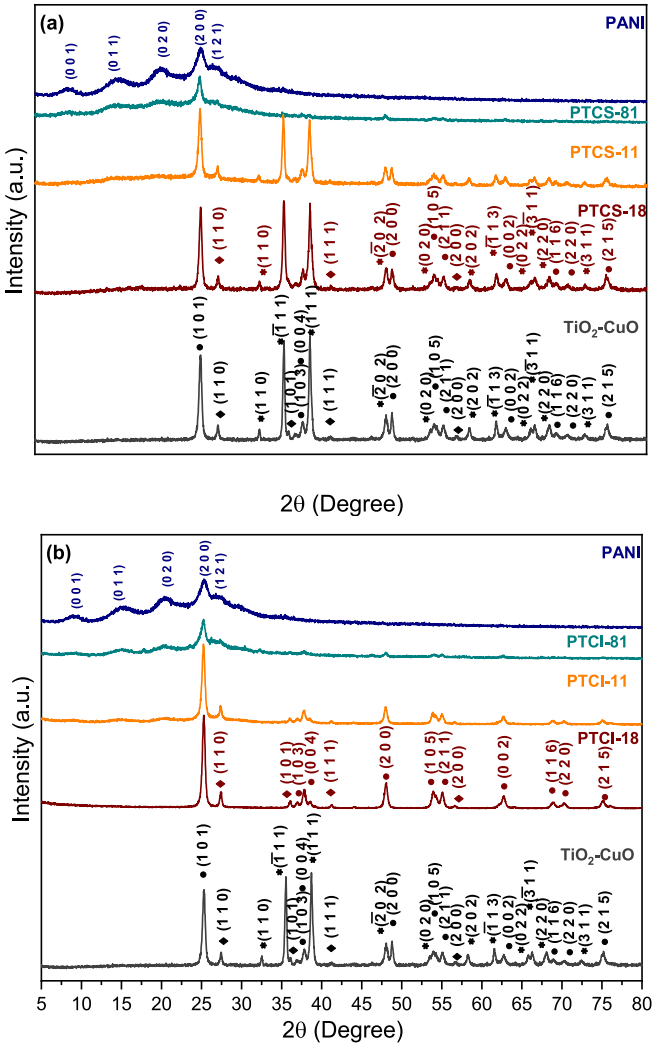

Fig. 1. XRD diffractograms for (a) PANI, PTCS-PANI composites, and TiO_2-CuO, (b) PANI, PTCI-PANI composites, and TiO_2-CuO (•anatase TiO_2, ◆rutile TiO_2, and *CuO).

The XRD diffractogram of the PTCS-PANI composites exhibited crystal planes of TiO_2, CuO, as well as PANI. This situation could be proven by incorporating metal oxides into the PANI matrix and confirming a ternary composite formation. The XRD pattern of PTCS-PANI composites revealed that the (2 0 0) and (1 2 1) planes of PANI overlapped with the (1 0 1) and (1 1 0) planes of anatase and rutile TiO_2, respectively. The intensities of characteristic diffraction peaks associated with TiO_2 and CuO decreased as the amount of PANI increased. Furthermore, it was observed that the broadness of XRD peaks for both TiO_2 and CuO, particularly in PTCS-81, was increased. The results were in good agreement with the successful preparation of PTCS-PANI composites.

Likewise, the peak intensities of TiO_2 revealed a gradual decrease as the amount of PANI increased in PTCI-PANI composites. For the ternary PTCI-PANI composites, the XRD pattern presented only the diffraction peaks of PANI and TiO_2 with no observable characteristic peaks of CuO. The reason for the disappearance of CuO signal was related to the dissolution of CuO and the release of Cu^{2+} ions under highly acidic conditions [29]. This indicates that either the Cu species were amorphous or highly dispersed on PANI [30] or complete elimination occurs

after dissolution. Similar results were obtained in our previous study [10]. The crystallite sizes of PANI, TiO_2-CuO, PTCS-PANI, and PTCI-PANI composites were estimated by using Sherrer's equation (Eq. (1)), and the calculated values were summarized as in SM, Part II, in Table S1. For the calculation of crystallite size in PANI-TiO_2 composites, the most significant anatase TiO_2 plane, (1 0 1), was selected; however, this highly intense plane overlapped with the semi-crystalline (2 0 0) plane of PANI. Therefore, the anatase (200) plane was chosen to calculate the crystallite sizes of the composites and to prevent any possible misinterpretation. The crystallite sizes for binary TiO_2-CuO composite and ternary PANI-TiO_2-CuO composites, specifically concerning the (1 0 1) plane, ranged from approximately 16 nm–21 nm, and their size was notably higher than that of PANI (~11 nm).

3.2. FTIR-ATR analysis

FTIR-ATR spectra of PANI, TiO_2-CuO, PTCS-PANI, and PTCI-PANI composites are shown in Fig. 2. The main peaks of PANI at 1585 cm^{-1} and 1481 cm^{-1} related to the C=N and C=C stretching modes of the quinonoid and benzenoid rings, respectively [31]. The peaks at 1296 cm^{-1} and 1242 cm^{-1} were attributed to the C-N stretching and C–$N^{+\bullet}$ stretching vibrations, respectively. The intense peak at 1110 cm^{-1} could belong to the vibrational modes of either Benzenoid–NH^+ = Quinone or Benzenoid–$NH^{+\bullet}$–Benzenoid charged units [32,33]. The peaks located in the 900 cm^{-1}-700 cm^{-1} region were associated with the aromatic ring and out-of-plane C–H deformation vibrations [34].

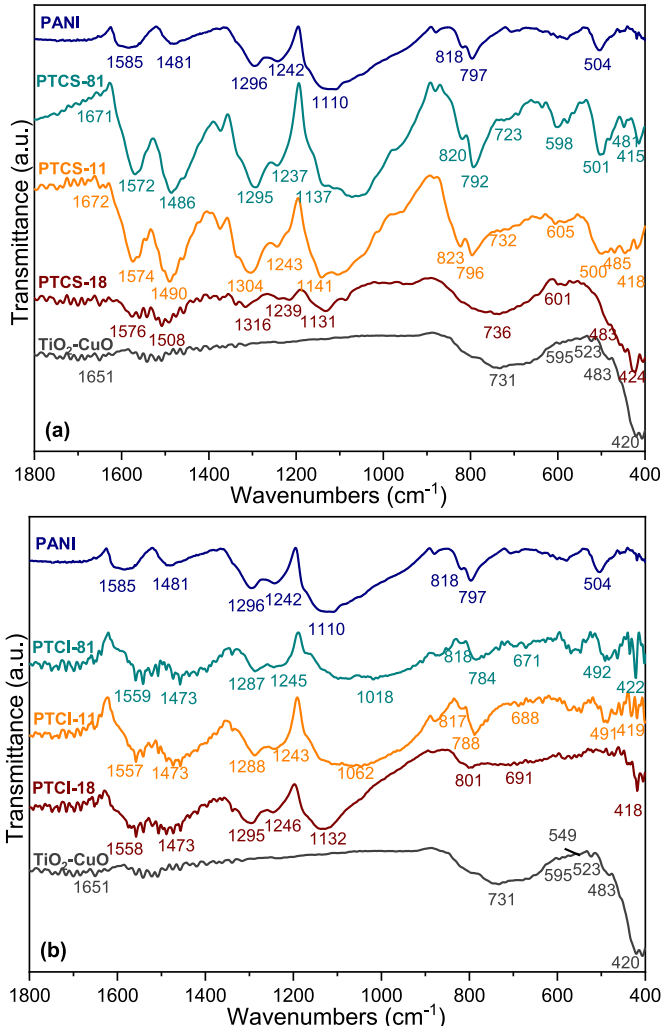

Fig. 2. FTIR-ATR spectra for (a) PANI, PTCS-PANI composites, and TiO_2-CuO, (b) PANI, PTCI-PANI composites, and TiO_2-CuO.

FTIR-ATR spectrum of TiO_2-CuO revealed a weak peak at 1651 cm^{-1}, belonging to the bending mode of the O-H groups, resulting from absorbed water on the surface. FTIR-ATR spectrum of CuO exhibited a weak peak at 1651 cm^{-1}, corresponding to the bending vibration (O-H group) of absorbed water on the surface. The observed peaks at 731 cm^{-1} and 420 cm^{-1} were attributed to the O–Ti–O and Ti-O bonding vibrations, respectively, while the peaks at 595 cm^{-1}, 523 cm^{-1}, and 483 cm^{-1} belonged to the stretching vibrations of the Cu-O bond of monoclinic CuO [35,36].

FTIR-ATR spectra of PTCS-PANI composites revealed the characteristic peaks of both PANI and TiO_2-CuO (Fig. 2 (a)). The peaks related to quinonoid (1585 cm^{-1}) and benzenoid (1481 cm^{-1}) rings of PANI shifted to 1572 cm^{-1} and 1486 cm^{-1} in the spectrum of PTCS-81 composite, respectively. These notable shifts in the vibrational frequencies could imply the presence of an electrostatic interaction between PANI and TiO_2-CuO [37]. As the amount of CuO increased, the peaks indicating the quinonoid and benzenoid ring structures in the PTCS-81 composite shifted to higher wavenumbers, and their intensities gradually decreased. For PTCS-81, the peaks at 1295 cm^{-1}, 1237 cm^{-1}, 1137 cm^{-1}, 820 cm^{-1}, and 792 cm^{-1} belonged to PANI. The peaks observed at 598 cm^{-1} and 481 cm^{-1} were attributed to CuO, while the observed peaks at 723 cm^{-1} and 415 cm^{-1} corresponded to TiO_2. The spectrum of PTCS-11 and PTCS-18 composites exhibited a general shift toward higher frequency peaks.

PTCI-PANI composites exhibited only the main vibrations of PANI and TiO_2 features, which varied in peak locations and intensities (Fig. 2 (b)). However, CuO signals were not detected in PTCI-PANI composites. It is worth noting that CuO is unstable in an acidic environment, leading to its dissolution and the release of Cu^{2+} ions [29]. This result agrees with the report on preparing PANI-CuO composites using HCl and yielding the obtained post-preparation [10]. The splitting of the intense peak at 1110 cm^{-1}, which is due to the doping of PANI, was commonly explained by the pseudoprotonation of the imine nitrogens by the metal cations, such as Cu^{2+} [38]. However, PTCS-PANI composites also showed similar behavior, so the behavior observed here in PTCI-PANI composites could not be interpreted as strong evidence for the presence of Cu^{2+} ions in the matrix.

3.3. SEM analysis

SEM images of PANI, TiO_2-CuO, PTCS-PANI, and PTCI-PANI composites are shown at two different magnifications (x100000 and x50000) in Figs. 3 and 4. SEM images of TiO_2 and CuO are presented in SM, Part II, in Fig. S1.

For morphological comparison, SEM images of PANI and binary TiO_2-CuO specimens are presented in Figs. 3 (a) and Fig. 4(a)–and Fig. 4 (e) and 4 (e), respectively. PANI was found to have a uniform distribution of large globule-shaped particles of varying sizes. SEM image corresponded to a binary TiO_2-CuO composite that exhibited a combination of a diversity of polyhedral-shaped CuO and nearly spherical particle-shaped TiO_2.

SEM image of ternary PTCS-81 composite (Fig. 3 (b)) revealed the dominant morphological feature of PANI, which contained a small loading of TiO_2-CuO composite on its surface. An increase in the binary TiO_2-CuO amount in the PTCS-11 composite (Fig. 3 (c)) resulted in an almost identical morphology among the ternary components of PANI, TiO_2, and CuO. As the highest TiO_2-CuO amount was reached in the PTCS-18 composite (Fig. 3 (d)), the morphology transformed into a stacked PANI in a binary TiO_2-CuO composite.

SEM images of ternary PTCI-PANI composites exhibited a binary morphology comprising PANI and TiO_2 components. SEM image of the PTCI-81 composite (Fig. 4 (b)) nearly maintained the globular morphology of PANI, which was complemented with a minor TiO_2 closely resembling that of PANI. Increasing the loading of binary TiO_2-CuO did not significantly alter the composite morphology compared to

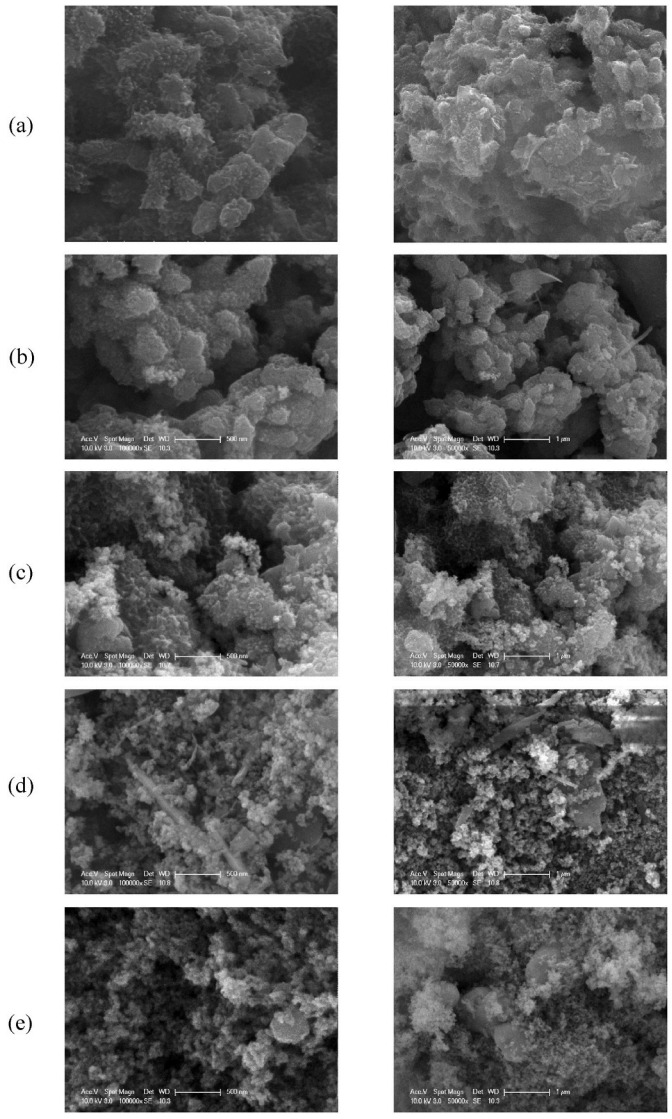

Fig. 3. SEM images (left) ×100000 and (right) ×50000 of (a) PANI, (b) PTCS-81, (c) PTCS-11, (d) PTCS-18, and (e) TiO_2-CuO.

PANI (Fig. 4 (c)). It was observed that PANI was primarily observed to be encapsulated around the spherical TiO_2 particles, and the number of bunches of TiO_2 increased in the PTCI-11 composite. However, the surface morphology of the PTCI-18 composite (Fig. 4 (d)) was remarkably changed, and TiO_2 partially covered the polymer matrix. It was observed that PANI particles in the composite were heaped more loosely than pure TiO_2 nanoparticles. This observed a loose cotton-like morphology due to the dissolution of CuO in highly acidic conditions, which was consistent with the literature [10,39].

3.4. Thermogravimetric analysis

TG (thermogravimetry) analysis of PANI, PTCS-PANI, and PTCI-PANI composites are presented in Fig. 5. The initial weight loss of PANI at the temperature range between 50 °C and 120 °C was attributed to the loss of physically adsorbed water, and the endothermic peak at 79 °C was about 4.4 % (Fig. 5 (a)). The second weight loss in the thermogram, occurring between 165 °C and 360 °C, corresponded to the impurities, small-chain oligomers, and/or dopants, resulting in a total weight loss of 15.6 % at around 256 °C. A significant weight loss in the 405 °C–675 °C range was related to the decomposition of PANI backbone and chains with an additional weight loss of 23.3 % at 526 °C. The first stage of PANI carbonization appeared in a nitrogen atmosphere at around 700 °C, leading to a total weight loss of 52.7 % [10].

TG and DTG (derivative thermogravimetry) of PTCS-PANI composites revealed a more stable and well-ordered decomposition nature than PANI (Fig. 5(b)–(c)). PTCS-81 showed the first weight loss step at around 90 °C, attributed to the release of water, was about 5 %. The following observed total weight loss step at 260 °C, belonging to the loss of dopants, was 11.9 %. The final thermal decomposition step at 501 °C resulted in a total weight loss of 52.7 %, which corresponded to the decomposition of the polymer, confirming the incorporation of the PANI matrix into binary TiO_2-CuO composite [40]. A gradual decrease in thermal decomposition was observed for PTSC-11 and PTCS-18 composites. For comparison, the total weight losses of PANI, PTCS-81, PTCS-11, and PTCS-18 were about 52.7 %, 41.8 %, 39.7 %, and 18.4 %, respectively.

TG and DTG curve profiles of all three different amounts of TiO_2-CuO loaded PTCI-PANI composites are presented in Fig. 5(d)–(e). Among PTCI-PANI composites, the weight loss percentage of the ternary PTCI-81 composite (49 %) was maximized, resembling that of PANI. The weight loss observed at approximately 261 °C was related to the removal of dopants, while the significant weight loss after 510 °C resulted from the breakdown of polymer chains. In addition, a comparison of the PTCI-11 and PTCI-18 composites revealed that they exhibited higher stability than the PTCI-81 composite. The TG curve of PTCI-11 indicated a sharp weight loss between 120 °C and 600 °C of temperature range (23.9 %) due to the well-ordered thermal decomposition nature of the polymer, and the total weight loss of ternary PTCI-11 was about 33.9 %. The ternary PTCI-18 composite exhibited the most stable thermogram curve with a total weight loss of only 22.7 %.

3.5. BET analysis

The surface features of PANI, TiO_2-CuO, and PTCS-PANI composites were determined using nitrogen adsorption-desorption isotherms (SM, Part II, Fig. S2), and all hysteresis curves were classified according to IUPAC standards [41]. PANI isotherm curve exhibited a type III curve trend, while the isotherm curves of binary TiO_2-CuO and ternary PTCS-PANI composites belonged to type IV characteristics with an H4 loop, indicating the presence of narrow slit pores [42].

The major BET surface output parameters of PANI, TiO_2-CuO, and PTCS-PANI composites are listed in SM, Part II, Table S2. Based on the acquired data, the BET surface areas of PANI and TiO_2-CuO were obtained as 26 m^2/g and 32 m^2/g, respectively. The ternary PTCS-81 composite, as the primary component of the PANI, exhibited the highest specific surface area of 37 m^2/g among the PTCS-PANI composites, potentially exposing additional activated sites favorable for the adsorption of reactive molecules. Incorporating TiO_2-CuO into the polymer matrix caused a gradual augmentation in the surface area of PTCS-PANI composites. It was noted that the surface areas of PTCS-11 (31 m^2/g) and PTCS-18 (21 m^2/g) composites were lower than that of PTCS-81. The pore sizes of PTCS-PANI composites were within the complete characteristics range of mesoporosity (20 Å-50 Å) and consistent with SEM analysis [41].

3.6. Photocatalytic activity

The photocatalytic activity tests of ternary PANI-TiO_2-CuO composites were conducted using a series of PTCS-PANI composites with three different ANI ratios, as CuO was not detected in PTCI-PANI composites due to its dissolution issues. Among PTCS-PANI composites, the PTCS-11 composite was also chosen as a representative specimen with equal amounts of ANI and TiO_2-CuO for the reusability studies and DFT calculations. The reproducibility of the results was determined to be less than 5 % through preliminary experiments conducted in triplicate before the main experimental part.

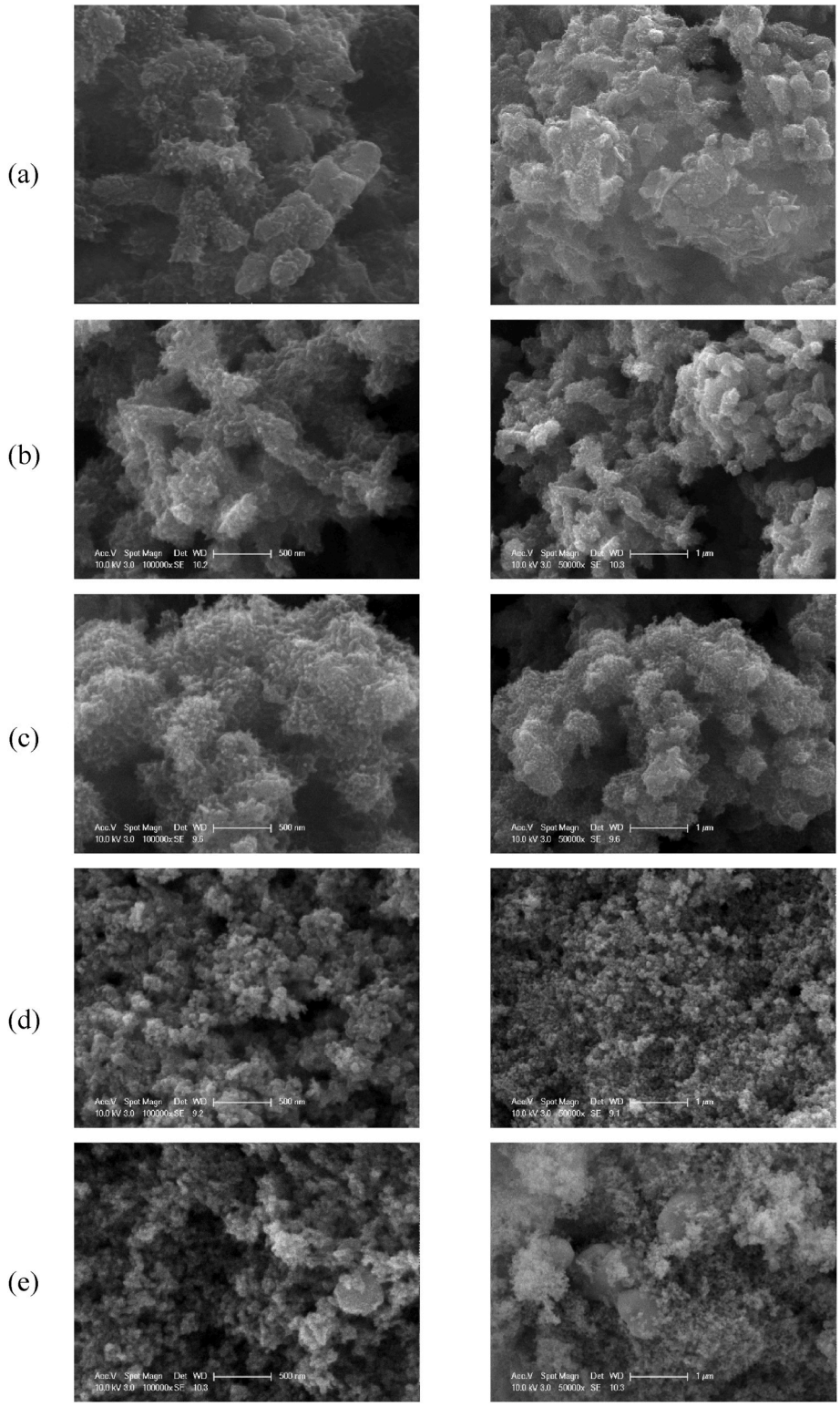

Fig. 4. SEM images (left) ×100000 and (right) ×50000 of (a) PANI, (b) PTCI-81, (c) PTCI-11, (d) PTCI-18, and (e) TiO_2-CuO.

3.6.1. Photocatalytic degradation of RB-198

The alterations in the UV–vis profile of RB-198 were analyzed using binary TiO_2-CuO and ternary PTCS-PANI composites (SM, Part III, Fig. S3). The initial spectrum of RB-198 exhibited a maximum absorption band at $\lambda_{max} = 625$ nm, corresponding to the chromophoric azo (−N=N−) bond in the visible region, and two other bands observed at $\lambda = 225$ nm and $\lambda = 266$ nm could be associated with the aromatic groups [10,43]. A gradual reduction in the intensity of these three absorption bands was noted as the reaction time increased. Nearly complete disappearance of the maximum band at $\lambda_{max} = 625$ nm was only observed using PTCS-81 composite within 60 min photocatalytic reaction time. This could indicate that the chromophore contains fragments from the cleavage of the azo bond. In contrast, a remarkably slower and gradually decreasing trend in the intensities of the visible band was

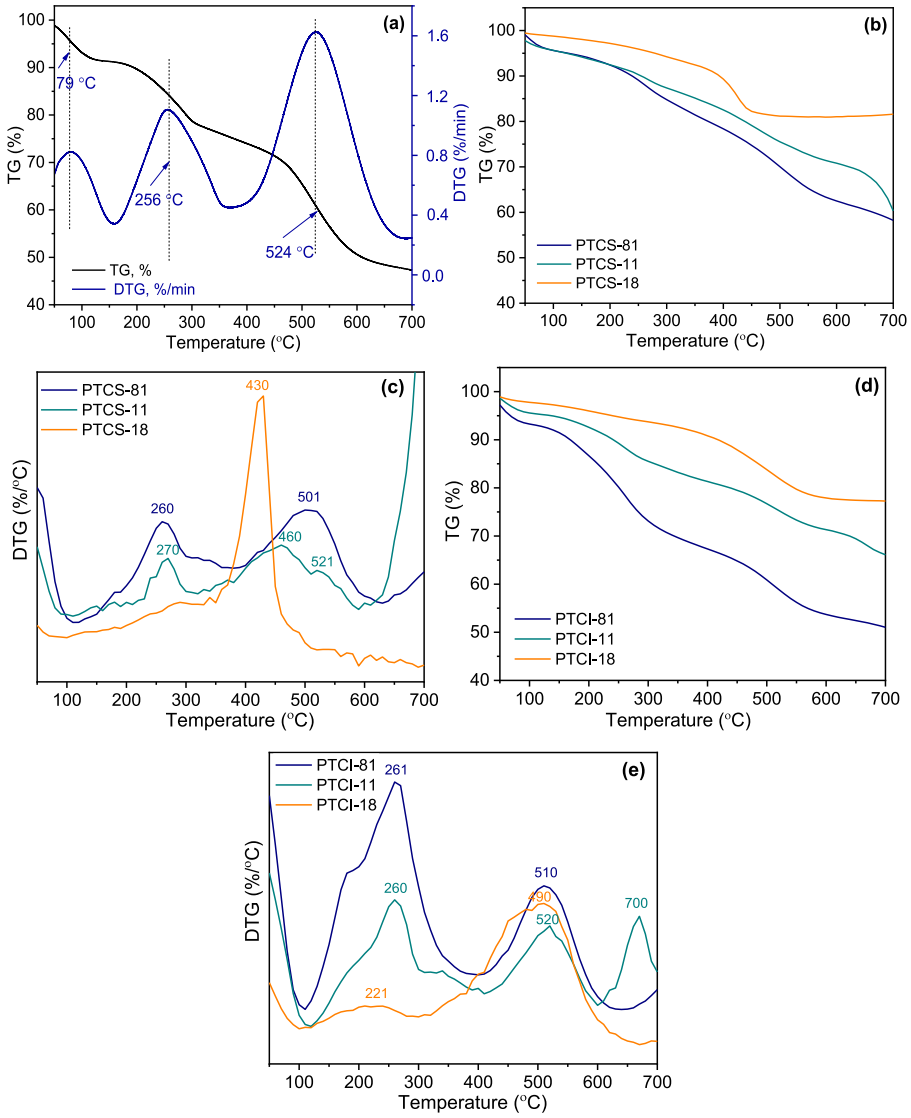

Fig. 5. (a) TG and DTG curves of PANI, (b) TG and (c) DTG curves of PTCS-PANI composites, and (d) TG and (e) DTG curves of PTCI-PANI composites.

observed in the presence of PTCS-18 and PTCS-11 composites.

The efficiency of photocatalytic decolorization of RB-198 was evaluated using binary TiO_2-CuO and ternary PTCS-PANI composites at various time intervals (Fig. S4) Among ternary PTCS-PANI composites, the PTCS-81 composite exhibited the highest photocatalytic activity for the decolorization of RB-198, achieving 90.4 % in 60 min, which was significantly higher than that of the binary TiO_2-CuO composite (65.1 %). The efficient degradation could be related to the electrostatic forces between anionic RB-198 dye and positively charged composite surface. pH_{pzc} values of PANI, TiO_2, and CuO were $pH_{pzc} = 7.3$, $pH_{pzc} = 5.7$, and $pH_{pzc} = \sim 8.5$, respectively [10,44]. Further increasing the TiO_2-CuO loading in PTCS-PANI composites decreased the photocatalytic decolorization efficiencies of PTCS-11 and especially PTCS-18.

The photocatalytic decolorization efficiency of TiO_2-CuO and PTCS-PANI composites on azo RB-198 dye was found to be in the following order:

PTCS-81>TiO_2-CuO > PTCS-11>PTCS-18.

The pseudo-first-order kinetic model parameters RB-198 using TiO_2-CuO and PTCS-PANI composites ($R^2 > 0.75$) were calculated by Eq. (3), and the results were presented in Table 1. The logarithmic decay profiles of composites are presented in SM, Part III, Fig. S5.

$$Rate\ (R) = \ln A_0/A = kt \quad (3)$$

Table 1
Photocatalytic degradation kinetic parameters RB-198 in the presence of binary TiO_2-CuO and ternary PTCS-PANI composites.

	First-order kinetic parameters		
Specimens	**$kx10^{-3}$, min^{-1}**	**$t_{1/2}$, min**	***Rate*, min^{-1}**
PTCS-81	65.7	10.55	0.0134
PTCS-11	3.68	188.4	0.0007
PTCS-18	2.77	250.2	0.0006
TiO_2-CuO	10.3	67.30	0.0021

where R is the pseudo first-order rate (min^{-1}), A_o and A_t are the absorbances of RB-198 at the initial and irradiation time t (min), respectively.

The half-life ($t_{1/2}$, min) could be calculated by using the pseudo first-order reaction rate constant (k, min^{-1}) according to the equation:

$$t_{1/2} = 0.692/k \quad (4)$$

The trend of photocatalytic degradation rate constants of composites could be expressed in decreasing order:

PTCS-81>TiO_2-CuO > PTCS-11>PTCS-18.

The ternary PTCS-81 composite exhibited a photocatalytic

degradation rate almost six times greater than the binary TiO_2-CuO in degrading RB-198 dye. The presence of PANI in the binary TiO_2-CuO composite reduces the recombination of photo-generated charges, resulting in increased photocatalytic activity of the ternary PTCS-81 composite [11]. As the amount of TiO_2-CuO increased, the values of rate constants decreased and were found to be $3.68x10^{-3}$ and $2.77x10^{-3}$ for PTCS-11 and PTCS-18 composites, respectively. It is well known that a high surface area contributed to the presence of surface hydroxyl groups, improving photocatalytic efficiency [10,45]. These outcomes could be verified by the surface areavalues of composites reported in Table S2.

3.6.2. Reusability and recyclability

The reusability and stability of the ternary PTCS-11 composite (0.25 g/L) were investigated by reusing the catalyst for the photodegradation of RB-198 (20 mg/L) for four consecutive cycles. The PTCS-11 composite was collected by centrifugation, washed with distilled water, and dried at 80 °C before being used for the upcoming cycles of the recycling test. The photodegradation activity of the recycled and reused PTCS-11 composite remained nearly as efficient as in the initial cycle, maintaining a conversion efficiency of 85 % by the fourth cycle (Fig. S6). A slight decrease in photocatalytic efficiency was observed in each cycle, which was attributed to insufficient photocatalyst dosage or loss during the washing process. The issue could arise from the inactivation of active sites and aggregation due to the following heating process [46].

To confirm the structural changes, the FTIR-ATR spectra of the PTCS-11 composite were recorded before and after each cycle of reaction (Fig. S7). The spectrum of the adsorbed RB-198 dye on the ternary PTCS-11 (denoted as t = 0) was closely identical to the shape and position of the spectrum from the unused PTCS-11. Furthermore, the FTIR-ATR recycled spectra remained unchanged throughout successive photocatalytic processes, confirming a stable catalyst. The XRD diffractograms of the unused PTCS-11 composite and the recovered catalyst were analyzed to identify any potential changes in their crystalline nature, in which it was observed that the crystallinity of PTCS-11 composite remained nearly unchanged, even after undergoing the fourth consecutive cycle (Fig. S8).

3.6.3. Probable photocatalytic degradation mechanism and silico toxicity of degradation products of RB-198

The optimized geometry of RB-198 is presented in SM, Part IV, Fig. S9, via computational calculations. Using Fukui functions, the potential photocatalytic degradation mechanism of RB-198 over the ternary PTCS-11 composite was determined. In addition, the photodegradation process was analyzed using FTIR-ATR and SEM, providing structural and morphological insights into the degradation process.

FTIR-ATR analysis was utilized to observe the structural changes in functional groups over various time intervals throughout the photocatalytic degradation of RB-198 (Fig. S10). FTIR-ATR spectra of PTCS-11 and adsorption of RB-198 on PTCS-11 (t = 0) are also presented in Fig. S11 for comparison. For the ternary PTCS-11 composite, the peaks at 1574 cm^{-1}, 1490 cm^{-1}, 1304 cm^{-1}, 1243 cm^{-1}, 1141 cm^{-1}, 823 cm^{-1} and 796 cm^{-1} related to PANI, whereas the peaks located at 1672 cm^{-1}, 732 cm^{-1}, 605 cm^{-1}, 485 cm^{-1}, 418 cm^{-1}, and 500 cm^{-1} corresponded to the binary TiO_2-CuO. After the adsorption of RB-198 dye onto the PTCS-11 composite (t = 0), the peak positions and intensities were slightly altered. A novel peak at 1640 cm^{-1} could represent the combined vibrations of the phenyl ring and the C=N group, and the peak at 1492 cm^{-1} was attributed to the stretching of the −N=N− bond of RB-198 or the characteristic PANI vibration. The intensity of the nitrogen group decreased gradually with increasing photocatalytic reaction time. The remaining chromophore group could be evidence of incomplete decolorization in the UV degradation profile of PTCS-11, as shown in Fig. S3 (b). As a result, a longer irradiation time was necessary to mineralize the azo dye completely.

The morphological alterations before and after the photocatalytic degradation processes were analyzed by SEM (Fig. S11). SEM image of the ternary PTCS-11 composite was also presented for comparative purposes. The adsorption of RB-198 dye onto the PTCS-11 composite resulted in a surface coverage and a smoother catalyst surface. After 120 min of photocatalytic degradation, the SEM image of the PTCS-11 composite revealed a distribution of spherical and polyhedral-shaped particles, particularly highlighting the morphological features of both PANI and the binary TiO_2-CuO composite.

Based on the DFT calculations, Fukui function indices were performed to determine the most probable reactive sites of RB-198 dye for hydroxyl radicals (•OH). Hence, higher f° indices indicated the atoms affected by •OH attacks. The theoretical parameters, such as local softness (s°), Fukui function (f°) indices, and softness difference (Δs°) values, were calculated, and the selected values responsible for •OH radical attacks were summarized in SM, Part IV, Table S3. It should be highlighted that the computed softness values were close to those of •OH at specific sites of the identified dye molecule. Moreover, the calculated Δs° values between the reacting atoms should be minimized [10,20].

Fig. 6 presents a proposed degradation pathway of RB-198 based on theoretical calculations and experimental data. According to Table S3, the highest Fukui indices values for nitrogen atoms confirm the most reactive sites of the RB-198 dye to the attack by •OH. The primary •OH attack focused on the two competitive pathway reactions by cleaving the azo bond (−N=N−) and the neighboring single C−N bond, which was in accordance with the reported earlier studies [18,21]. In our case, the highest Fukui indices (f^0) values were N33 and N39 atoms belonging to the azo and amino moiety groups, respectively, and suggested that the azo bond cleavage mechanism was favored over these atom groups simultaneously. The azo and amino group bond cleavage mechanism for the photocatalytic degradation of RB-198, at the same time, leading to the formation of fragment (I) and fragment (II).

Pathway I: The first pathway of the degradation process took place simultaneously, where the most reactive atoms were N33 and N39 atoms in the azo and amino moiety groups, respectively. Initially, the •OH attack on the (−N=N−) bond formed fragment (I) and could be degraded to compound (1). N35 and N39 in the azo group, and the cleavage of this chromophore group could indicate discoloration. Subsequent to the •OH attack on N35 underwent two pathways with the loss of the amino group, denoted as pathway I (a) and pathway I (b), resulting in the breakdown to compounds (2) and (3). Compound (2) was split into a sodium ethyl sulfate group attached to the benzene moiety (4) and triazine moiety (7) that could proceed with the loss of a sodium ethyl sulfate group, ultimately resulting in the formation of low-weight compounds. Afterward, the photocatalytic process could degrade these compounds into CO_2 and H_2O. Similarly, the compound (3) could undergo the loss of sulfonate group (10), then convert to compound (11). Subsequently hydroxylated, the ring-opening reaction could take place, and further could mineralize into CO_2 and H_2O. The degradation compounds were mostly in accordance with previously reported studies [21,47].

Pathway II: Pathway II began with the •OH attacking the C-N bond, resulting in the formation of fragment (II), which was then converted to compound (12). Following the radical attack at the second azo position (N18 and N19), which were attached to both the naphthalene moiety and the phenyl ring, the compounds (13) and (14) could result. In the next step, compound (13) could be oxidized to compound (15), then could undergo cleavage of the sodium sulfonate groups attached to the naphthalene ring (compound (16)). This compound (16) could further mineralize into small molecules. In the case of pathway II (b), the removal of chromophore group could form compound (14), and oxidize to compound (17). The loss of sulfonate group could generate compound (18). The final product (19) was ultimately formed through a process of ring-opening and mineralization. Similar results were reported in literature [21,48]. Furthermore, CDFT calculations supported the experimental results from UV–vis and FTIR-ATR analyses, indicating a gradual decrease in the spectral bands of both aromatic and chromophore

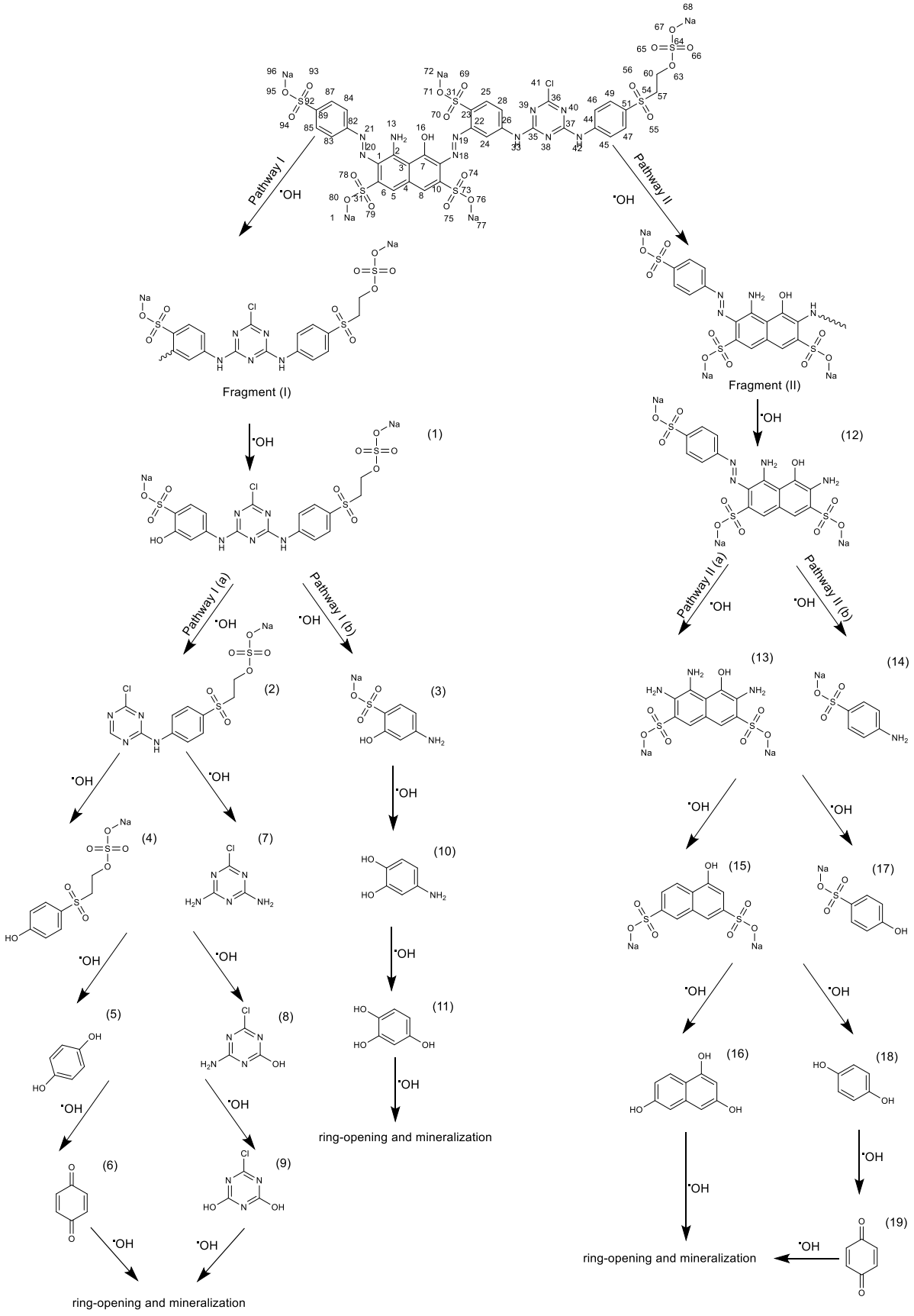

Fig. 6. Proposed photocatalytic degradation mechanism of RB-198.

groups.

Computational tools were employed to predict the silico toxicological effects of the degraded products, and the results were presented in Table S4. In accordance with the ProTox 3.0 classification steps, the carcinogenicity, immunotoxicity, mutagenicity, and cytotoxicity of possible degraded products were assessed. RB-198 diazo dye fell under relatively harmless (predicted toxicity class 6) and stimulated activity in hepatoxicity, nephrotoxicity, respiratory toxicity, carcinogenicity, and the blood-brain (BBB) barrier. The degradation compounds in this study, such as compounds ((6) and (19)) were found to be active for significantly carcinogenic (predicted toxicity class 2), three compounds ((5), (8), and (11)) were found to be active in terms of carcinogenic effect (predicted toxicity class 3), while five compounds ((8), (9), (10), (16), and (17)) were slightly toxic (predicted toxicity class 4). According to our results, compounds ((1), (2), (4), (7), (14), and (15)) were determined as non-mutagenic predicted toxicity class 5) and compound (12) as mutagenic (predicted toxicity class 5), whereas the compounds ((3), and (13)) were relatively harmless.

Among the degraded compounds, the predicted median lethal dose (LD_{50}) analysis highlighted that 1,4-benzoquinone (compounds (6) and (19)) could pose the highest risks (LD_{50} = 25 mg/kg). Compounds (3) and (13) were predicted to have a low toxicity profile at high LD_{50}, indicating they were environmentally friendly. It is well known that 1,4-benzoquinone is a benzene metabolite, associated with genotoxic and mutagenic effects [49]. It was reported that the acute toxicity LD_{50} values of 1,4-benzoquinone were 464 mg/kg [50], 320 mg/kg [51], and a small LD_{50} = 8.5 mg/kg [49]. Moreover, hydroquinone (compounds (5) and (18)) exhibited a significantly lower LD_{50} (225 mg/kg) value. Topping et al. reported that the LD_{50} value was higher than 375 mg/kg in male rats and 367.3 mg/kg in female rats [52]. In another experimental toxicity study, the oral-rat LD_{50} value of hydroquinone was found to be 320 mg/kg [50]. These values were similar to the predicted LD_{50} value, a quantitative criterion of acute toxicity. In conclusion, the photocatalytic degradation of RB-198 resulted in most of the degraded compounds still maintaining slightly toxic, non-mutagenic, and relatively harmless toxicity levels. However, some degraded products were classified as significantly carcinogenic, carcinogenic, and mutagenic, particularly those with low LD_{50} values.

In further studies, we plan to conduct a comparative study on the proposed degradation products of RB-198 using analytical techniques to fully identify the degraded intermediates experimentally.

4. Conclusions

This study presented the synthesis and comparative characterization of ternary PANI-TiO_2-CuO composites via *in-situ* chemical oxidation polymerization and mechano-chemical techniques. It was found that the ratio of PANI and binary TiO_2-CuO influenced the structural and morphological characteristics of ternary composites. XRD diffractograms indicated the presence of semi-crystalline PANI, as well as crystalline TiO_2 and CuO planes in the PTCS-PANI composites. In contrast, the PTCI-PANI composites only exhibited PANI and TiO_2 planes, while CuO was not detected due to its dissolution issues. SEM images of PTCI-PANI composites supported the XRD data, particularly for the PTCI-18 composite, which revealed a looser morphology compared to pure TiO_2 nanoparticles.

The photocatalytic results indicated that PTCS-81 achieved a removal rate of RB-198 of up to 90.4 % within 60 min. The reusability of the ternary composites revealed a slight decrease in RB-198 degradation, maintaining an impressive efficiency of 85 % after four cycles. Recycling and reuse tests further emphasized the efficiency and stability of PANI-TiO_2-CuO composites as promising catalysts in photocatalytic processes.

CDFT calculations were employed to determine that the regioselectivity of •OH attack was more probable based on local reactivity descriptors. Reactivity descriptors identified the susceptible sites in the diazo dye that are reactive to hydroxyl radical attack, as determined by Fukui functions. Fukui indices were calculated to elucidate the predictable photocatalytic degradation mechanism of RB-198 with the combination of experimental data. The higher Fukui function indicated the most sensitive sites for •OH attack on N33 and N39, identifying the most reactive atoms. Additionally, CDFT calculations confirmed the experimental findings from UV–vis and FTIR-ATR analyses, where the spectral bands of both aromatic compounds and chromophores revealed a gradual decline. Silico toxicity studies highlighted the degradation products of RB-198, particularly concerning sustainable industrial practices, raising concerns about whether their incomplete mineralization of azo dyes could pose an actual threat to the environment.

The findings of PANI-TiO_2-CuO composites offer valuable insights into the practical application and design of the photocatalytic degradation reactions for efficiently removing azo dyes. Understanding all aspects of the potential photocatalytic degradation mechanism and predicting the silico toxicological effects of degraded products of RB-198 could significantly reduce environmental and health risks associated with water treatment processes.

CRediT authorship contribution statement

Nazli Turkten: Writing – review & editing, Methodology, Investigation, Formal analysis. **Yunus Karatas:** Writing – review & editing, Supervision, Methodology, Investigation, Conceptualization. **Simal Kurumoglu:** Writing – original draft, Software, Investigation. **Yelda Yalcin Gurkan:** Writing – review & editing, Software, Investigation.

Statement of Novelty

The manuscript covers significant and novel information on combined experimental and theoretical investigations conducted for the first time on the ternary PANI-TiO_2-CuO composite, considering the gap in p-n-p type photocatalytic performance. This study also highlighted the preparation and detailed characterization of ternary PANI-TiO_2-CuO composites through *in-situ* chemical oxidation polymerization and mechano-chemical synthesis methods for comparison. For the first time, the theoretical and experimental proposal for the photocatalytic mechanism of Reactive Blue 198 was conducted to describe the predicted reaction pathways, and theoretical findings were supported by experimental spectral results and literature. Additionally, the reusability and recycling properties of ternary PANI-TiO_2-CuO composites were investigated. Finally, the silico toxicity of potential photodegraded products of Reactive Blue 198 was conducted via the computational toxicology method ProTox-3.0 to assess the toxicity of predicted compounds.

Declaration of competing interest

The authors declare that they have no known competing financial interests or personal relationships that could have appeared to influence the work reported in this paper.

Acknowledgments

The financial support provided by Tekirdag Namik Kemal University BAP unit through Project No. NKUBAP. 01.GA.25.666 and NKUBAP.64. GA.25.656 is gratefully acknowledged.

Appendix A. Supplementary data

Supplementary data to this article can be found online at https://doi.org/10.1016/j.physb.2025.417802.

Data availability

Data will be made available on request.

References

[1] W.U. Khan, S. Ahmed, Y. Dhoble, S. Madhav, A critical review of hazardous waste generation from textile industries and associated ecological impacts, J. Indian Chem. Soc. 100 (1) (2023) 100829.

[2] H. Dhila, A. Bhapkar, S. Bhame, Metal oxide/biochar hybrid nanocomposites for adsorption and photocatalytic degradation of textile dye effluents: a review, Desalin.Water Treat. 321 (2025) 101004.

[3] J.A. Oyetade, R.L. Machunda, A. Hilonga, Photocatalytic degradation of azo dyes in textile wastewater by polyaniline composite catalyst-a review, Sci. Afr. 17 (2022) e01305.

[4] S. Khan, T. Noor, N. Iqbal, L. Yaqoob, ACS omega "Photocatalytic Dye Degradation from Textile Wastewater, A Review 9 (20) (2024) 21751–21767.

[5] N. Turkten, Y. Karatas, M. Bekbolet, Conducting polymers and photocatalysis: a mini review on selected conducting polymers and photocatalysts as TiO_2 and ZnO, Journal of Photocatalysis 2 (4) (2021) 252–270.

[6] M. Sajith, H. S, S. Sambhudevan, A comprehensive review on photocatalytic degradation of textile dyes using PANI-Semiconductor composites, Water Air Soil Pollut. 235 (9) (2024) 594.

[7] N.K. Jangid, S. Jadoun, A. Yadav, M. Srivastava, N. Kaur, Polyaniline-TiO_2-based photocatalysts for dyes degradation, Polym. Bull. 78 (8) (2021) 4743–4777.

[8] N. Turkten, Y. Karatas, C.S. Uyguner-Demirel, M. Bekbolet, Preparation of PANI modified TiO_2 and characterization under pre- and post- photocatalytic conditions, Environ. Sci. Pollut. Res. 30 (51) (2023) 111182–111207.

[9] N. Turkten, Y. Karatas, M. Bekbolet, Preparation of PANI modified ZnO composites via different methods: structural, morphological and photocatalytic properties, Water 13 (8) (2021).

[10] N. Turkten, Y. Karatas, Y.Y. Gurkan, New insights into the application of copper-based polymer composites as Catalysts: an Indepth experimental and computational study, Inorg. Chem. Commun. 174 (2025) 113919.

[11] R. Nekooie, T. Shamspur, A. Mostafavi, J. "Novel CuO/TiO_2/PANI nanocomposite: preparation and photocatalytic investigation for chlorpyrifos degradation in water under visible light irradiation", Photochem. Photobiol. 407 (2021) 113038.

[12] O. Koysuren, H.N. Koysuren, Application of CuO and its composite with polyaniline on the photocatalytic degradation of methylene blue and the Cr(VI) photoreduction under visible light, J. Sol. Gel Sci. Technol. 106 (1) (2023) 131–148.

[13] H.N. Koysuren, O. Koysuren, Photocatalytic activity of boron doped CuO and its composite with polyaniline, Polymer-Plastics Technol. Mat. 62 (3) (2023) 281–293.

[14] B.S. Rathore, N.P.S. Chauhan, M.K. Rawal, S.C. Ameta, R. Ameta, Chitosan–polyaniline–copper(II) oxide hybrid composite for the removal of methyl orange dye, Polym. Bull. 77 (9) (2020) 4833–4850.

[15] T.B. Gelaw, B.K. Sarojini, A.K. Kodoth, Chitosan/Hydroxyethyl cellulose Gel immobilized Polyaniline/CuO/ZnO adsorptive-photocatalytic hybrid nanocomposite for Congo red removal, J. Polym. Environ. 30 (10) (2022) 4086–4101.

[16] M.A.A. Borik, M.A. Diab, H.A. El-Sabban, A.-B.A.A.M. El-Adasy, M.S.A. El-Gaby, Designed construction of boosted visible-light Z-scheme TiO_2/PANI/Cu_2O heterojunction with elaborated photocatalytic degradation of organic dyes, Synth. Met. 306 (2024) 117642.

[17] S. Rajendran, R. Pachaiappan, T.K.A. Hoang, S. Karthikeyan, L. Gnanasekaran, S. Vadivel, M. Soto-Moscoso, M.A. Gracia-Pinilla, CuO-ZnO-PANI a lethal p-n-p combination in degradation of 4-chlorophenol under visible light, J. Hazard. Mater. 416 (2021) 125989.

[18] A.S. Özen, V. Aviyente, R.A. Klein, Modeling the oxidative degradation of Azo dyes: a density functional theory Study, J. Phys. Chem. A 107 (24) (2003) 4898–4907.

[19] R. Pino-Rios, E. Pino, G. Cárdenas-Jirón, Deciphering the origin of the first steps in the degradation of azo dyes: a computational study, Environ. Sci. Pollut. Res. 31 (1) (2024) 657–667.

[20] Y.Y. Gurkan, N. Turkten, A. Hatipoglu, Z. Cinar, Photocatalytic degradation of cefazolin over N-doped TiO_2 under UV and sunlight irradiation: prediction of the reaction paths via conceptual DFT, Chem. Eng. J. 184 (2012) 113–124.

[21] N. Turkten, Z. Cinar, Photocatalytic decolorization of azo dyes on TiO_2: prediction of mechanism via conceptual DFT, Catal. Today 287 (2017) 169–175.

[22] M. Mohammadi, S. Sabbaghi, H. Sadeghi, M.M. Zerafat, R. Pooladi, Preparation and characterization of TiO_2/ZnO/CuO nanocomposite and application for phenol removal from wastewaters, Desalination Water Treat. 57 (2) (2016) 799–809.

[23] P. Scherrer, Nachr Ges, Wiss Gottingen, Estimation of the size and internal structure of colloidal particles by means of röntgen 2 (1918) 96–100.

[24] M.J. Frisch, G.W. Trucks, H.B. Schlegel, G.E. Scuseria, M.A. Robb, J.R. Cheeseman, G. Scalmani, V. Barone, G.A. Petersson, H. Nakatsuji, X. Li, A.M.M. Caricato, B.G.J. J. Bloino, R. Gomperts, B. Mennucci, H.P. Hratchian, J.V. Ortiz, A.F. Izmaylov, J. L. Sonnenberg, D. Williams-Young, F. Ding, F. Lipparini, F. Egidi, J. Goings, B. Peng, T.H.A. Petrone, D. Ranasinghe, V.G. Zakrzewski, J. Gao, N. Rega, G. Zheng, W. Liang, M. Hada, M. Ehara, K. Toyota, R. Fukuda, J. Hasegawa, M. Ishida, T. Nakajima, Y. Honda, O. Kitao, H. Nakai, K.T.T. Vreven, J. A. Montgomery, J.E. P, Jr, F. Ogliaro, M. Bearpark, E.B.J.J. Heyd, K.N. Kudin, V. N. Staroverov, R.K.T. Keith, K.R.J. Normand, A. Rendell, J.C. Burant, S.S. Iyengar, J. Tomasi, M. Cossi, J.M. Millam, M. Klene, C. Adamo, R. Cammi, J.W. Ochterski, R.L. Martin, K. Morokuma, O. Farkas, J.B. Foresman, a.D.J. Fox, Gaussian 09, Revision A.02, Gaussian, Inc., Wallingford CT, 2016.

[25] A.D. Becke, Density-functional thermochemistry. III. The role of exact exchange, J. Chem. Phys. 98 (7) (1993) 5648–5652.

[26] M.J. Frisch, J.A. Pople, J.S. Binkley, Self-consistent molecular orbital methods 25. Supplementary functions for Gaussian basis sets, J. Chem. Phys. 80 (7) (1984) 3265–3269.

[27] P. Banerjee, E. Kemmler, M. Dunkel, R. Preissner, ProTox 3.0: a webserver for the prediction of toxicity of chemicals, Nucleic Acids Res. 52 (W1) (2024) W513–W520.

[28] J. Stejskal, A. Riede, D. Hlavatá, J. Prokeš, M. Helmstedt, P. Holler, The effect of polymerization temperature on molecular weight, crystallinity, and electrical conductivity of polyaniline, Synth. Met. 96 (1) (1998) 55–61.

[29] H. Fu, S. Shewfelt, L.D. Sylvan, J.-F. Gaillard, K.A. Gray, Polyaniline-metal oxide coatings for biocidal applications: mechanisms of activation and deactivation, Chemosphere 346 (2024) 140543.

[30] Y. Chen, Q. Zhang, X. Jing, J. Han, L. Yu, Synthesis of Cu-doped polyaniline nanocomposites (nano Cu@PANI) via the H_2O_2-promoted oxidative polymerization of aniline with copper salt, Mater. Lett. 242 (2019) 170–173.

[31] Y. Deng, L. Tang, G. Zeng, H. Dong, M. Yan, J. Wang, W. Hu, J. Wang, Y. Zhou, J. Tang, Enhanced visible light photocatalytic performance of polyaniline modified mesoporous single crystal TiO_2 microsphere, Appl. Surf. Sci. 387 (2016) 882–893.

[32] M. Trchová, J. Stejskal, Polyaniline: the infrared spectroscopy of conducting polymer nanotubes (IUPAC Technical Report), Pure Appl. Chem. 83 (10) (2011) 1803–1817.

[33] Z. Ping, J. Chem Soc, In situ FTIR–attenuated total reflection spectroscopic investigations on the base–acid transitions of polyaniline. Base–acid transition in the emeraldine form of polyaniline, Faraday Trans. 92 (17) (1996) 3063–3067.

[34] J. Stejskal, I. Sapurina, "Polyaniline — a conducting polymer, in: U. Schubert, N. Hüsing, R.M. Laine (Eds.), Materials Syntheses: a Practical Guide, Springer Vienna, Vienna, 2008, pp. 199–207.

[35] K. Borgohain, J.B. Singh, M.V. Rama Rao, T. Shripathi, S. Mahamuni, Quantum size effects in CuO nanoparticles, Phys. Rev. B 61 (16) (2000) 11093–11096.

[36] A. Kapoor, Pratibha, J.K. Rajput, Solar light photocatalytic activity of CuO/TiO_2 mixed oxide derived from conjugated azomethine metal complex for degradation of food colorants, J. Mol. Liq. 366 (2022) 120280.

[37] P. Singh, S.K. Shukla, Structurally optimized cupric oxide/polyaniline nanocomposites for efficient humidity sensing, Surf. Interfaces 18 (2020) 100410.

[38] H. Xu, J. Zhang, Y. Chen, H. Lu, J. Zhuang, Electrochemical polymerization of polyaniline doped with Cu^{2+} as the electrode material for electrochemical supercapacitors, RSC Adv. 4 (11) (2014) 5547–5552.

[39] R. Ullah, S. Bilal, K. Ali, A.-u.-H.A. "Synthesis and characterization of polyaniline doped with Cu II chloride by inverse emulsion polymerization", Shah, Synth. Met. 198 (2014) 113–117.

[40] N. Boutaleb, F.Z. Dahou, H. Djelad, L. Sabantina, I. Moulefera, A. Benyoucef, Facile synthesis and electrochemical characterization of Polyaniline@TiO_2-CuO ternary composite as electrodes for supercapacitor applications, Polymers 14 (21) (2022) 4562.

[41] K.S.W. Sing, Reporting physisorption data for gas/solid systems with special reference to the determination of surface area and porosity (recommendations 1984), Pure Appl. Chem. (1985) 603.

[42] S. Yurdakal, C. Garlisi, L. Özcan, M. Bellardita, G. Palmisano, Chapter 4 - (photo) catalyst characterization techniques: adsorption isotherms and BET, SEM, FTIR, UV–Vis, photoluminescence, and electrochemical characterizations, in: G. Marcì, L. Palmisano (Eds.), Heterogeneous Photocatalysis, Elsevier, 2019, pp. 87–152.

[43] T. Kanagaraj, S. Thiripuranthagan, S.M.K. Paskalis, H. Abe, Visible light photocatalytic activities of template free porous graphitic carbon nitride—BiOBr composite catalysts towards the mineralization of reactive dyes, Appl. Surf. Sci. 426 (2017) 1030–1045.

[44] N. Turkten, Z. Cinar, A. Tomruk, M. Bekbolet, Copper-doped TiO_2 photocatalysts: application to drinking water by humic matter degradation, Environ. Sci. Pollut. Res. Int. 26 (36) (2019) 36096–36106.

[45] S. Safa, R. Azimirad, S. Safalou Moghaddam, M. Rabbani, Investigating on photocatalytic performance of CuO micro and nanostructures prepared by different precursors, Desalination Water Treat. 57 (15) (2016) 6723–6731.

[46] R. Riaz, I. Bibi, F. Majid, S. Kamal, M.A. Huwayz, K. Jilani, A. Ghafoor, Q. Raza, N. Alwadai, M. Iqbal, $NiFe_2O_4$/CuO heterostructures optical, magnetic and photocatalytic properties: methylene blue dye degradation under solar light irradiation, J. Mol. Struct. 1309 (2024) 138174.

[47] M.B. Nguyen, G.H. Le, T.D. Nguyen, Q.K. Nguyen, T.T.T. Pham, T. Lee, T.A. Vu, Bimetallic Ag-Zn-BTC/GO composite as highly efficient photocatalyst in the photocatalytic degradation of reactive yellow 145 dye in water, J. Hazard. Mater. 420 (2021) 126560.

[48] T.H. Bokhari, A. Naveed, M.K. Khosa, A.u. Haq, M. Muneer, M. Iqbal, O. A. Mohammed, A.S. Doghish, M.A. Abdel-Reheim, M. Iqbal, A. Nazir, By-product distribution and cytotoxicity assessment of ZnO-assisted photocatalytic degradation of reactive blue 250 dye, Heliyon 10 (22) (2024) e39670.

[49] M. Bedner, W.A. MacCrehan, Transformation of Acetaminophen by chlorination produces the toxicants 1,4-Benzoquinone and N-Acetyl-p-benzoquinone imine, Environ. Sci. Technol. 40 (2) (2006) 516–522.

[50] Q. Zhang, Y.-L. Yang, Z. Huang, Y.-y. Liu, J.-m. Hong, Stability and reactivity improved bimetallic 2D metal organic frameworks for electrocatalytic degradation of p-acetaminophenol, Environ. Chem. Eng. 11 (5) (2023) 110734.

[51] A. Akyol, Toxicity assessment and degradation of benzoquinone by ZnO photocatalytic oxidation process, Desalin.Water Treat. 137 (2019) 202–211.

[52] D.C. Topping, L.G. Bernard, J.L. O'Donoghue, J.C. English, Hydroquinone: acute and subchronic toxicity studies with emphasis on neurobehavioral and nephrotoxic effects", Food Chem. Toxicol. 45 (1) (2007) 70–78.